scientific reports

Check for updates

OPEN

Evidence for the early Toarcian Carbon Isotope Excursion (T-CIE) from the shallow marine siliciclastic red beds of Arabia

Mahmoud Alnazghah[1], Ardiansyah Koeshidayatullah[2,3]✉, Abdulkarim Al-Hussaini[1], Abduljamiu Amao[3], Haijun Song[4] & Khalid Al-Ramadan[2,3]

The Toarcian Oceanic Anoxic Event (T-OAE) and its corresponding Carbon Isotope Excursion (CIE) have been reported widely across the Tethyan region and globally. In Arabia, and based on ammonite dating, the time window of the T-OAE coincided with the deposition of the reddish siliciclastic unit of the Marrat Formation. However, no evidence of the T-OAE/CIE was ever reported from Arabia because these red beds were previously interpreted as continental deposits. Recently, these red beds have been recognized as shallow marine deposits which opened an opportunity to assess the occurrence and expression of T-OAE–CIE in Arabia. In this study, a multiproxy geochemical characterization was performed on the Toarcian Marrat Formation to infer the chemistry of the paleowater column and identify intervals of possible T-OAE/CIE in Arabia. While the low concentrations of redox-sensitive elements (Mo, U, V, Cr) may indicate a shallow oxic marine settings, the coupled negative $\delta^{13}C_{organic}$ excursion and apparent increase in the chemical weathering suggests that the deposition of Marrat red beds coincided with the development of T-CIE and possibly time-equivalent to the T-OAE globally. The origin of reddening is interpreted to have occurred during the middle Marrat deposition due to the stabilization of unstable hydrous iron oxides to hematite under oxic marine conditions. The proposed model further indicates the possible development of source rocks in the deep, anoxic environment counterpart where the T-OAE may be expressed. Since our study documents the first record of the T-CIE and discuss the origin of shallow marine siliciclastic red beds in the Arabian Plate, this will have significant implications for the overall understanding of the T-CIE globally and for hydrocarbon exploration through realizations of potential new source rocks associated with the OAEs in the Toarcian and other time intervals.

The Toarcian Oceanic Anoxic Event (T-OAE) is one of the key biogchemical events across the geological record. Previous studies have argued that the T-OAE was triggered by the emplacement of the Karoo Large Igneous Province coupled with the release of carbon from climate-sensitive reservoirs (e.g., gas hydrates, wet lands, permafrost soil), causing severe environmental perturbations[1–7]. Environmental perturbations (such as carbon cycle perturbation, increasing pCO_2, and global warming) caused major faunal extinctions during this time interval[3,7–16]. While the global extent of the T-OAE was questioned because most datasets were documented from the epicontinental seas of northwestern Europe[5,9–11], other studies highlighted the occurrences of time-equivalent negative Carbon Isotope Excursion (CIE) across the Tethys and Panthalassa oceans, advocating the global nature of the T-OAE[17–19]. Globally, the T-OAE is marked by a major negative carbon excursion of $\delta^{13}C_{organic}$ and $\delta^{13}C_{carbonate}$[3], within carbonate strata[20], and fossil wood[4]. Most of the previous research on the T-OAE focused on deep marine black shales and their time-equivalent shallow-water carbonate facies[2,3,11]. However, recent studies show a consistent occurrence of deep and shallow marine red beds during and after the onset of marine

[1]Exploration Organization, Saudi Aramco, Dhahran, Saudi Arabia. [2]Department of Geosciences, College of Petroleum Engineering and Geosciences, King Fahd University of Petroleum and Minerals, Dhahran, Saudi Arabia. [3]Center for Integrative Petroleum Research, College of Petroleum Engineering and Geosciences, King Fahd University of Petroleum and Minerals, Dhahran, Saudi Arabia. [4]State Key Laboratory of Biogeology and Environmental Geology, China University of Geosciences, Wuhan, China. ✉email: a.koeshidayatullah@kfupm.edu.sa

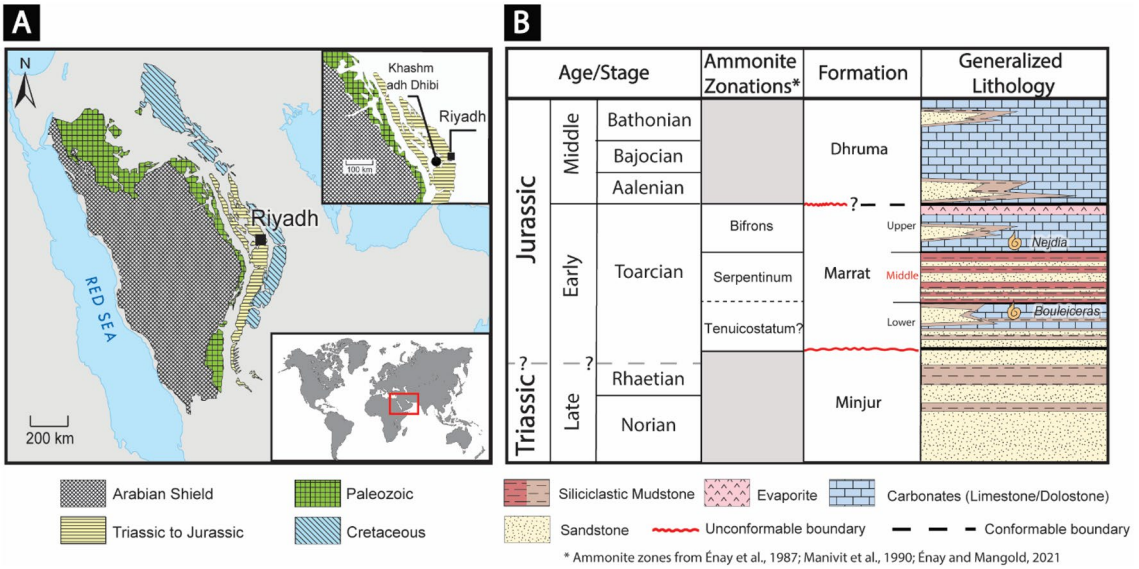

Figure 1. (**A**) Geological map showing the location of the Khashm adh Dhibi outcrop where the stratigraphic section was measured and sampled[35]. (**B**) Generalized stratigraphic column of the Late Triassic—Early Jurassic in Saudi Arabia.

anoxia across the geologic record, significantly increasing the importance of these red beds as possible indicators of OAE's[21–26].

Although the ammonite dating of the Marrat carbonates of Arabia constrains the age of the middle Marrat siliciclastic red beds to be within the time window of the T-OAE (Fig. 1)[27–29], no documentation or attempts have been made to investigate whether this globally recognized event had extended to Arabia. This can possibly be explained by the fact that these red beds have long been viewed as continental deposits[30–34] with the assumption that they cannot yield important geochemical results that can be used for correlation with the reported T-OAE/CIE data from the nearby Tethyan basins. Recently, however, a revised interpretation of these red beds indicated that these red beds were deposited under shallow-marine settings[35], providing a unique opportunity to assess, for the first time, the possible extent of the T-OAE/CIE across the Arabian Plate and the possibility of using shallow marine siliciclastic red beds as an indicator of OAEs or CIE. Therefore, this study aims to (i) assess whether the T-OAE/CIE event influenced the Arabian Plate and (ii) reveal whether there is any record that can be attributed to environmental changes associated with the T-OAE/CIE through systematically conducting high-resolution multiproxy geochemical characterizations of the Marrat Formation. The outcomes of this study are expected to help enhance the global understanding of the T-OAE/CIE and how this event is represented in shallow-marine siliciclastic deposits.

Geological settings and study area

During the late Permian to early Triassic, the Zagros rifting had a profound impact on the Arabian Plate and the sedimentary architecture of its Mesozoic strata[36,37]. The opening of the Neo-Tethys ocean, as a result of the Zagros rifting, had resulted in the development of an ENE-dipping passive margin along the northeastern margin of the Arabian Plate[36–38]. In addition to the Zagros-related ENE passive margin, another N-dipping Neo-Tethys passive margin was formed along the northern edges of the Arabian Plate due to the Early Jurassic back-arc rifting in the eastern Mediterranean[36–38]. The Early Jurassic Marrat Formation is forming a discontinuous, N-S oriented, arc-shaped outcrop belt that can be traced for more than 650 km in central Arabia, with a total thickness that ranges between 111 and 142 m[30,31]. It has an unconformable contact with the underlying Triassic Minjur Formation, while the upper contact with the overlying Dhruma Formation is generally found to be conformable[30,31,39–41]. However, some published articles suggest that the Marrat-Dhruma contact is unconformable in some places[30,31,34,42,43]. Previously conducted studies on the Marrat Formation divided its deposits into three lithological units; lower, middle and upper[30,31,39,40,42,44–46]. The lower Marrat consists of siliciclastic deposits at the base that transition vertically into carbonates, while the upper Marrat unit is mainly composed of carbonates and anhydrites[30,31,35,39,40,42,44,45]. The middle Marrat is consistently made of reddish mudstones (claystone) with intercalations of sandstone and siltstone[30,31,35,39,40,42,44–46]. The lower and upper Marrat carbonates are replaced by siliciclastics deposits towards the southern parts of the outcrop (towards the updip direction)[30,31].

The ammonite dating of the Marrat carbonates constrains the age of the middle Marrat red beds to be within the *serpentinum* ammonite zone of the early Toarcian[27–29,47]. The lower Marrat carbonates, where the *Bouleiceras* and *Protogrammoceras* faunas were found, are assigned to be representing the upper part of the *Tenuicostatum* zone to the lower part of the *Levisoni* (or *Serpentinum*) zone of the Mediterranean and northwest European scales[27,29]. For the upper Marrat carbonates, the identified *Nejdia* fauna is suggesting middle Toarcain age (*Sublevisoni* Subzone of the *Bifrons* Zone)[27,29].

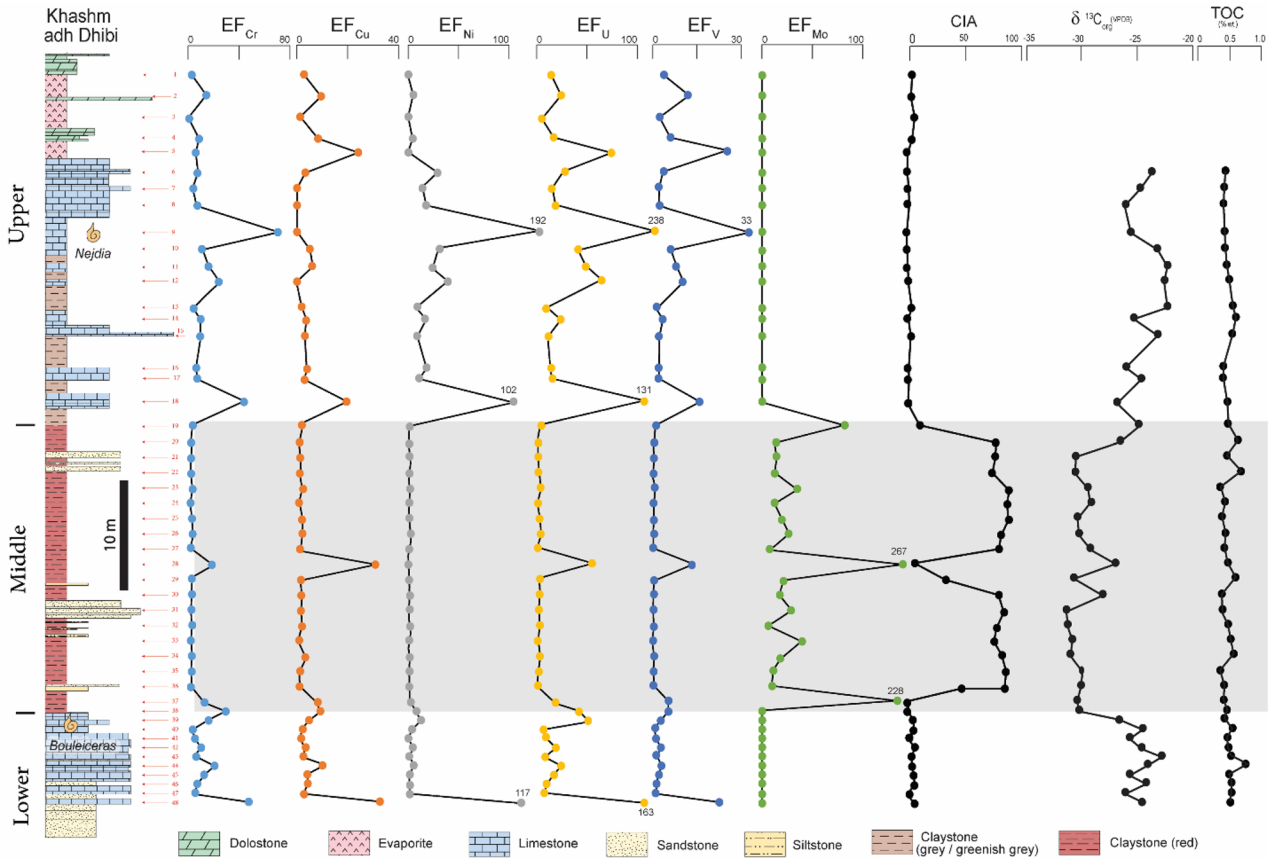

Figure 2. The measured section of the Marrat Formation in Khashm adh Dhibi with sample locations (red arrows) with plots of the calculated enrichment factors (relative to average shale) of some redox sensitive elements (Cr, Cu, Ni, U, V, Mo), Chemical Index of Alteration (CIA), $\delta^{13}C_{org}$, and TOC. It is notable to highlight that the lowermost siliciclastic parts of the lower Marrat is not included in this measured section.

Even though the outcrops of the Marrat Formation are exposed at different localities, the Khashm adh Dhibi locality is considered to be the reference section due to the well-preserved exposures that it hosts[30,31,39]. Furthermore, the existence of detailed biostratigraphic (ammonite) analyses on the Khashm adh Dhibi section gives it a competitive advantage over the other Marrat sections[27,28,47]. Therefore, and based on the aforementioned objectives of our study, the Khashm adh Dhibi section (24°19′ 54″ N; 46°06′ 38″ E) was selected to be analyzed in this study.

Methods

A stratigraphic section of the Marrat Formation was measured at Khashm adh Dhibi, central Arabia (Figs. 1 and 2) and was sampled at approximately 1-m intervals for high-resolution elemental, mineral, Total Organic Carbon (TOC), and stable organic carbon isotope analyses. Prior to the Inductively Coupled Plasma (ICP) analysis, the collected samples were grounded to very fine powder (to less than 10 micron) using an agate grinder to avoid sample contamination, and then they were liquefied using the alkali fusion preparation technique. Here, 6 M hydrochloric acid (HCl) was used to dissolve the samples. In addition, 10 ml of de-ionized water were added into the solution to ensure that total dissolved solids will be less than 0.1%. The solutions were then further acidified by 2% HNO_3 and filtered to remove particles > 0.45 μm[48,49]. Elemental concentrations were measured using Agilent 7500ce Inductively Coupled Plasma Mass Spectrometry (ICP-MS), after using standard single- and multi-element references materials for calibration. Detection limits for this analysis is as low as 0.01 ppb in solution under the usual operating conditions. Mineralogical identification using X-ray Diffraction (XRD) was conducted using an InXitu BTX 308 XRD Analyzer. After isolating the organic matter from the collected samples through acid (HCl-HF) maceration, TOC and $\delta^{13}C_{org}$ ($\delta^{13}C$ of the organic matter) analyses were performed using a Costech 4010 Elemental Analyzer combustion system coupled with Thermo DeltaV Plus Isotopic Ratio Mass Spectrometer. The $\delta^{13}C_{org}$ values are reported in the Vienna Pee Dee Belemnite (VPDB) standard and have analytical precision of 0.1‰.

Results

Mineralogy. The Marrat red beds are composed primarily of phyllosilicate (up to 59%) and quartz (up to 99%) with an average of 17% and 32%, respectively, in addition to minor amounts of calcite and dolomite (< 5%). Additionally, notable increases in the contents of pyrite (up to 4.4%) and hematite (up to 8.1%) were observed

in the red beds. In contrast, the bounding carbonates are predominantly composed of calcite, constituting up to 99.3% of the rock volume, with minor amounts of quartz (< 3%), pyrite and hematite (< 1%).

Redox sensitive elements. Concentrations of some redox-sensitive elements (e.g., Cr, U, V, and Mo) were analyzed and normalized to aluminum across the Marrat Formation (Table 1 and supplementary material). In addition, enrichment factors (EF)[50] (to average shale[51]) were calculated for some of the redox-sensitive elements (Fig. 2) (detailed calculation and equation are available in the supplementary material). In general, similar trends are observed in the normalized redox-sensitive elements (Cr, U, and V) concentrations across the lower, middle, and upper units of the Marrat Formation where these elements are enriched in the upper and lower Marrat carbonates and no enrichment across the middle Marrat red beds (Table 1 and supplementary material). However, Molybdenum (Mo) is an exception where it shows an inverse signal to the aforementioned elements (Table 1). Across the middle Marrat red beds, the average normalized Cr, U, and V concentrations are 4.7, 0.07, and 11.9, respectively (Table 1). In contrast, the upper and lower carbonates show a significant enrichment (up to 7x) of these elements with average values of 15.9 and 16.9 for Cr, 0.37 and 0.19 for U, and 73.7 and 54.9 for V (Table 1).

Calculations of the EFs show that the lower and upper Marrat units have median EF of 10.33 and 8 for Cr, 2.29 and 3.96 for V, and 18.49 and 22.55 for U. In both the lower and upper Marrat units, EF Mo shows no enrichment. Across the middle Marrat, the median EFs of chromium, vanadium, uranium, and molybdenum are 2.91 (range 1.94–18.71), 0.55 (range 0.29–13.53), 4.07 (range 2.23–56.23), and 19.51 (range 6.13–266.70), respectively.

Alterations and weathering indicators. Several weathering indices, including (i) Chemical Index of Alteration (CIA)[52]; (ii) Chemical Index of Weathering (CIW)[53]; and (iii) Plagioclase index of Alteration (PIA)[54], were calculated to assess and quantify the degree and extent of weathering across the Marrat Formation (Fig. 2; supplementary material). Significant enrichment of these indicators, up to 2.5 orders of magnitude, was observed in the red beds when compared with the underlying and overlying carbonates. The red beds have a CIA ranging from 2.66 to 79.8 (mean: 59.67), PIA ranging from 0.01 to 95.2 (mean: 66.44), and CIW ranging from 2.73 to 96.5 (mean: 69.75) (Fig. 2). These values are much higher than those of the bounding carbonates. In fact, the carbonates exhibit consistently low values with very similar ranges across these three indicators, ranging from 0 to 3, with a mean value of approximately 1.

TOC and Paleoproductivity. The TOC content across the Marrat Formation is consistently below 1%, fluctuating between 0.31 and 0.9 wt.%. The average TOC across these sedimentary units is indistinguishable, 0.47 wt.% and 0.51 wt.% between the red beds and carbonate units, respectively (Fig. 2). Paleoproductivity tracers (Ba, Cu, Ni) were also analyzed and their enrichment factors were calculated. In the lower Marrat unit, the median of EF_{Ba}, EF_{Cu}, and EF_{Ni} are 3.46 (range 0–18.78), 4.04 (range 1.62–32.58), and 3.66 (range 0–117.29), respectively. Similar EF values for the respective elements were calculated for the upper Marrat unit where the medians of these elements were EF_{Ba} 3.40 (range 0–32.23), EF_{Cu} 3.16 (range 0–24.08), and EF_{Ni} 15.20 (range 0–192.32). For the middle Marrat unit, paleoproductivity trace elements exhibit an overall depletion trend compared to the upper and lower units. The median enrichment factors were EF_{Ba} 0.37 (range 0.13–41.17), EF_{Cu} 1.52 (range 0.76–30.78), and EF_{Ni} 1.08 (range 0–2.41).

Stable organic carbon isotope. The stable $\delta^{13}C_{org}$ values indicate a pronounced depletion (of up to −5‰) across the middle Marrat red beds relative to the upper and lower Marrat Carbonates. The $\delta^{13}C_{org}$ values are ranging between −31.17 to −25.16‰ (mean: −29.41‰) for the red beds, while the values across the carbonate units are ranging between −29.99 to −22.53‰ (mean: −24.78‰) (Fig. 2).

Discussion

First record of the T-CIE in Arabia. Several studies have reported the occurrence of negative carbon isotopic excursion (CIE), with a magnitude of −3‰ to −8‰, during the early Toarcian in both the Tethys and Panthalassa oceans (Fig. 3)[2,4–6,11,17–20,55–60]. This Toarcian-aged CIE marked a period of hyperthermal event coupled with the rapid expansion of marine oxygen-deficient areas with severe environmental perturbations[11,61]. Globally, the duration of the T-OAE is constrained between the *tenuicostatum* and *serpentinum* ammonite zones[4,19]. In Arabia, based on ammonite dating, this time interval was constrained to be within the Marrat Formation (Fig. 3)[27–29,45], suggesting that the Marrat red beds were deposited during the time window of the T-OAE.

However, the recognition of the T-OAE/CIE in Arabia has never been considered due to the traditional non-marine interpretation of these red beds[30–34], and the lack of $\delta^{13}C_{carb}$ and $\delta^{13}C_{org}$ records covering the early Toarcian succession of Arabia. Recently, the newly introduced shallow-marine interpretation for the Marrat red beds raises the necessity to investigate the potential occurrence of the T-OAE/CIE in Arabia[35].

Our multiproxy approach provides the first systematic geochemical records from the Arabian Toarcian succession. The $\delta^{13}C_{org}$ records a pronounced CIE, up to 5 ‰VPDB lighter than the bounding carbonates, across the Marrat red beds (Figs. 2 and 3). Based on the ammonite dating of the Marrat carbonates, this negative excursion falls entirely within the expected time window of the T-OAE (Fig. 2). The increase in various weathering indicators (CIA, PIA and CIW) suggests elevated CO_2 concentrations in the atmosphere and accelerated continental weathering possibly associated with volcanism during the emplacement of Karoo Igneous Province during the early Toarcian[18,65]. Invariance TOC values across this T-CIE zone may be explained by the low preservation potential of organic matter associated with a high-energy depositional environment and increased rate of siliciclastic influx diluting the organic carbon concentration. In fact, and as a result of the low TOC values, major changes in the organo-facies of the Marrat are highly unlikely to cause the negative CIE. Thus, the reported negative CIE within the middle Marrat may indeed reflect the global T-CIE.

Redox-sensitive elements (after AI normalization)							Enrichment Factor (to average shale)							Chemical and Weathering indices			Stable $^{13}C_{org}$ and TOC	
																	$^{13}C_{org}$	TOC
Ba/AI	Cr/AI	Cu/AI	Mo/AI	Ni/AI	U/AI	V/AI	EF (Ba)	EF (Cr)	EF (Cu)	EF (Mo)	EF (Ni)	EF (U)	EF (V)	CIA	PIA	CIW	VPDB	% wt
Upper Marrat carbonate																		
0.00	3.30	1.53	0.00	0.00	0.18	25.52	0.00	2.93	2.72	0.00	0.00	15.70	3.99	1.11	1.11	1.11		
27.31	16.12	5.32	0.00	4.22	0.56	41.49	3.77	14.33	9.45	0.00	4.96	25.53	12.14	0.82	0.82	0.82		
11.92	1.03	0.69	0.00	0.00	0.12	10.53	1.64	0.92	1.22	0.00	0.00	6.48	2.56	2.26	1.30	2.28		
5.67	9.70	4.64	0.00	3.71	0.29	29.44	0.78	8.62	8.25	0.00	4.37	18.12	6.25	1.00	0.65	1.00		
0.00	6.75	13.54	0.00	0.00	1.18	122.67	0.00	6.00	24.08	0.00	0.00	75.49	25.60	0.18	0.10	0.18		
91.89	8.28	1.83	0.00	24.59	0.18	47.82	12.67	7.36	3.26	0.00	28.93	29.43	3.92	0.29	0.23	0.29	−23.84	0.46
23.42	4.59	0.00	0.00	11.88	0.10	26.36	3.23	4.08	0.00	0.00	13.98	16.22	2.18	0.53	0.45	0.53	−24.91	0.44
47.24	8.27	0.00	0.00	15.04	0.12	32.52	6.52	7.35	0.00	0.00	17.69	20.01	2.52	0.48	0.35	0.48	−26.24	0.42
158.32	79.42	0.00	0.00	163.47	1.53	387.80	21.84	70.59	0.00	0.00	192.32	238.65	33.12	0.04	0.00	0.04	−25.76	0.44
0.00	12.26	2.80	0.00	26.46	0.29	69.08	0.00	10.89	4.99	0.00	31.13	42.51	6.28	0.21	0.02	0.21	−23.34	0.45
0.00	18.08	3.32	0.00	20.47	0.38	81.22	0.00	16.07	5.90	0.00	24.09	49.98	8.11	0.20	0.13	0.20	−22.51	0.50
32.13	27.16	0.00	0.00	33.23	0.48	106.86	4.43	24.14	0.00	0.00	39.09	65.76	10.34	0.14	0.29	0.14	−22.78	0.54
15.48	4.89	1.01	0.00	7.64	0.07	17.39	2.14	4.35	1.80	0.00	8.98	10.70	1.50	0.87	0.60	0.87	−22.53	0.60
59.00	11.14	2.01	0.00	13.96	0.16	40.76	8.14	9.90	3.57	0.00	16.43	25.08	3.54	0.46	0.43	0.46	−25.61	0.66
22.67	10.71	1.73	0.00	7.35	0.10	21.26	3.13	9.52	3.07	0.00	8.65	13.08	2.23	0.77	0.30	0.77	−23.41	0.59
25.83	7.22	2.23	0.00	15.33	0.10	25.53	3.56	6.42	3.96	0.00	18.03	15.71	2.17	0.63	0.44	0.63	−26.46	0.43
121.87	8.04	1.66	0.00	9.09	0.10	27.72	16.81	7.15	2.95	0.00	10.69	17.06	2.09	0.70	0.36	0.71	−24.92	0.43
233.68	49.51	10.95	0.00	87.54	0.75	213.11	32.23	44.01	19.47	0.00	102.99	131.14	16.13	0.08	0.04	0.08	−27.16	0.51
Middle Marrat red beds																		
15.05	4.20	1.06	2.67	1.15	0.06	9.67	2.08	3.74	1.89	82.12	1.35	5.95	1.32	5.07	3.70	5.15	−25.16	0.51
3.36	2.77	0.57	0.45	0.75	0.03	4.79	0.46	2.46	1.02	13.90	0.88	2.95	0.68	69.92	94.29	96.46	−26.85	0.69
2.65	2.67	0.69	0.46	0.92	0.03	4.71	0.37	2.37	1.23	14.13	1.08	2.90	0.55	65.10	72.46	77.86	−30.38	0.44
1.70	2.75	0.61	0.41	0.90	0.02	4.85	0.23	2.45	1.08	12.49	1.05	2.99	0.44	61.35	66.28	72.29	−30.40	0.69
4.90	4.03	1.34	1.13	1.45	0.04	8.36	0.68	3.58	2.38	34.85	1.71	5.14	0.84	77.79	82.22	83.53	−29.27	0.32
2.58	2.19	0.43	0.40	0.77	0.02	4.21	0.36	1.95	0.76	12.34	0.90	2.59	0.42	79.80	95.16	96.15	−28.96	0.41
2.83	3.44	1.09	0.63	0.80	0.02	6.62	0.39	3.06	1.93	19.51	0.94	4.07	0.53	79.43	88.26	89.80	−30.22	0.35
1.62	4.03	1.19	0.85	2.01	0.03	8.50	0.22	3.58	2.11	26.21	2.37	5.23	0.63	71.89	80.82	84.07	−30.08	0.41
1.15	2.40	0.64	0.24	0.66	0.01	3.96	0.16	2.14	1.14	7.52	0.78	2.44	0.30	69.17	77.79	81.87	−29.07	0.39
298.49	21.05	17.32	8.67	0.00	0.63	91.37	41.17	18.71	30.78	266.70	0.00	56.23	13.53	2.66	0.01	2.73	−26.73	0.46
15.26	3.28	0.86	2.64	0.59	0.03	7.44	2.10	2.91	1.52	81.29	0.69	4.58	0.62	19.90	18.17	20.45	−30.56	0.59
3.40	3.48	0.92	0.69	1.39	0.03	6.69	0.47	3.10	1.64	21.23	1.63	4.12	0.57	69.94	79.85	83.87	−27.90	0.35
1.91	2.96	0.84	0.57	1.08	0.02	5.61	0.26	2.63	1.50	17.59	1.28	3.45	0.43	74.48	83.31	85.86	−31.17	0.35
5.70	3.71	1.10	0.93	1.41	0.02	7.32	0.79	3.29	1.96	28.66	1.66	4.50	0.53	66.91	74.09	78.63	−31.04	0.45
0.93	2.42	0.48	0.20	0.68	0.01	3.62	0.13	2.15	0.85	6.13	0.80	2.23	0.29	62.46	66.04	70.31	−30.63	0.50
2.25	3.30	1.82	1.29	1.11	0.03	7.29	0.31	2.93	3.23	39.65	1.31	4.49	0.64	70.31	74.63	77.06	−30.82	0.55
1.92	3.22	0.70	0.58	0.98	0.02	5.59	0.27	2.86	1.25	18.00	1.15	3.44	0.48	77.05	86.59	88.60	−29.63	0.31
2.16	2.47	0.55	0.36	0.65	0.02	4.28	0.30	2.20	0.97	11.11	0.77	2.63	0.37	76.64	89.92	91.93	−29.82	0.38
35.84	14.57	4.59	7.40	2.05	0.26	32.53	4.94	12.95	8.16	227.64	2.41	20.02	5.57	33.91	28.77	38.59	−30.19	0.38
Lower Marrat carbonate																		
74.27	33.31	5.16	0.00	6.88	0.26	70.30	10.24	29.61	9.18	0.00	8.09	43.26	5.53	0.46	0.33	0.46	−29.99	0.43
83.84	18.16	2.66	0.00	10.70	0.13	85.11	11.56	16.14	4.73	0.00	12.59	52.37	2.91	0.46	0.14	0.46	−26.31	0.39
14.83	4.15	1.26	0.00	3.11	0.05	13.22	2.05	3.69	2.24	0.00	3.66	8.13	1.01	1.55	1.55	1.55	−24.15	0.53
0.00	6.11	0.91	0.00	0.00	0.06	17.06	0.00	5.43	1.62	0.00	0.00	10.50	1.29	1.85	1.81	1.85	−25.33	0.44
56.82	11.62	1.91	0.00	3.71	0.14	32.98	7.84	10.33	3.39	0.00	4.37	20.30	2.94	0.61	0.52	0.61	−24.24	0.46
33.59	7.14	1.40	0.00	0.67	0.06	15.86	4.63	6.35	2.49	0.00	0.78	9.76	1.35	2.64	1.82	2.66	−22.39	0.50
20.06	23.39	5.63	0.00	4.50	0.14	41.55	2.77	20.79	10.01	0.00	5.29	25.57	3.11	0.99	0.82	0.99	−23.67	0.76
25.07	14.16	2.27	0.00	1.26	0.11	30.05	3.46	12.58	4.04	0.00	1.48	18.49	2.29	1.22	0.64	1.23	−25.33	0.47
19.36	8.18	2.37	0.00	1.31	0.07	17.98	2.67	7.27	4.21	0.00	1.54	11.07	1.46	1.92	1.89	1.92	−23.83	0.51
15.43	6.36	1.53	0.00	1.19	0.06	14.39	2.13	5.65	2.72	0.00	1.40	8.86	1.22	2.32	1.49	2.34	−25.73	0.51
136.14	53.63	18.32	0.00	99.70	1.06	266.10	18.78	47.67	32.58	0.00	117.29	163.75	22.97	0.06	0.00	0.06	−24.21	0.49

Table 1. Geochemical analyses of the Marrat Formation. For display purposes, the Al-normalized concentrations are multiplied by 1000. For the raw concentration data, please check the supplementary material.

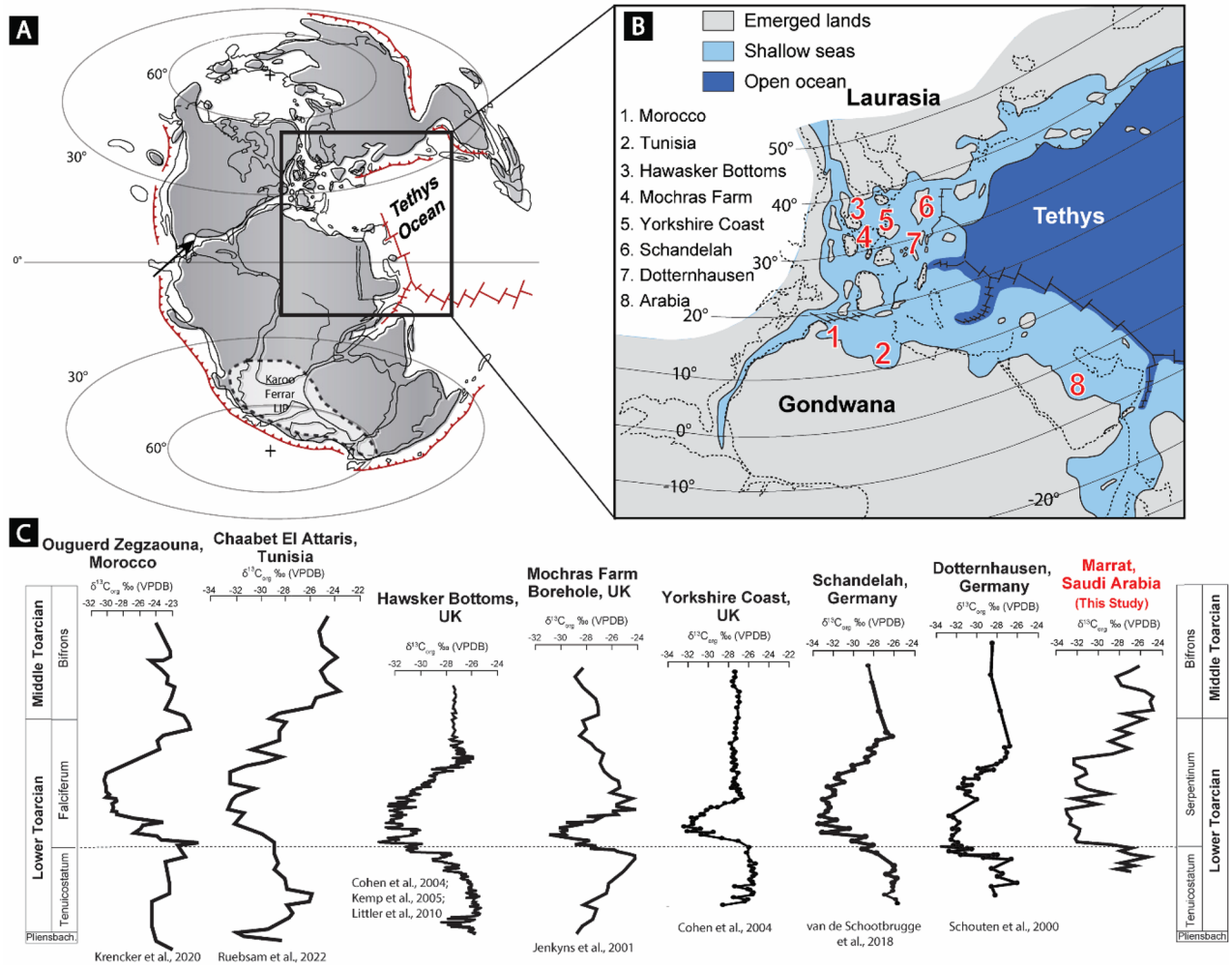

Figure 3. (**A**) Toarcian paleogeographic map of the world[62]. (**B**) Close-up paleogeographic map of the Western Tethyan realm showing the geographic location of Arabia relative to some localities where T-CIE was reported[20]. (**C**) Correlation between the $\delta^{13}C_{org}$ obtained from the Marrat Formation and the negative excursions in $\delta^{13}C_{org}$ reported from different basins within the Tethys[6,11,55–60,63,64].

Absence of redox-sensitive trace element enrichment. Enrichment in redox-sensitive trace elements (such as U, V, Ni, Cu, Mo, Cr) is widely considered as a signal for prevailing redox-conditions during oceanic anoxic events[50,66–74], however, several studies have highlighted examples for OAE's where CIE lacks coeval major enrichment in the redox-sensitive trace elements[18,75–78]. Erba et al.[75] indicate that the mean ocean residence time of many trace elements in the deep oceanic environments can be affected by biological and chemical processes, resulting in controlling the concentrations of these elements in the rock record. On the other hand, for the shallow marine environments with mixed siliciclastic and carbonate sediments, high-energy depositional settings (such as storms) and/or relatively high siliciclastic input are found to be hindering the development of prevailing oxygen-depleted conditions, resulting in the absence of trace-element enrichment[18,78]. The geochemical proxy data of Marrat red beds, except the enrichment factor of Mo, do not exhibit any signature of marine anoxia or increased primary productivity (Fig. 2), suggesting the prevalence of oxic conditions. The enrichment factor of Mo (EF_{Mo}) is only anomaly showing significant enrichment of trace elements across the Marrat red beds (Fig. 2). However, the significant enrichment in Mo with no coeval enrichment in U (Fig. 4) may point to particulate shuttle activity[79]. Shuttle of particulate Mo suggests that it is likely being scavenged by other phases in the sediment[80,81] accelerating the transfer of Mo into the sediment compared to other redox sensitive trace elements.

In general, the observed low concentrations and enrichment factors of redox-sensitive trace elements, along with the low preservation of organic matters, are likely related to the dynamic depositional settings and the elevated siliciclastic input during the middle Marrat time. This possibly had resulted in limiting the upwelling of the oxygen-depleted water to the shallow water settings where the Marrat was deposited along the outcrop. In addition, these findings suggest that marine anoxia is strongly controlled by local to regional basin conditions which make it regional-scale phenomena instead of global phenomena. This is evident from the prevailing development of black shales and marine anoxia in the northern areas of the Tethys shelf, while the southern parts of the shelf were dominated by oxic conditions[3,7].

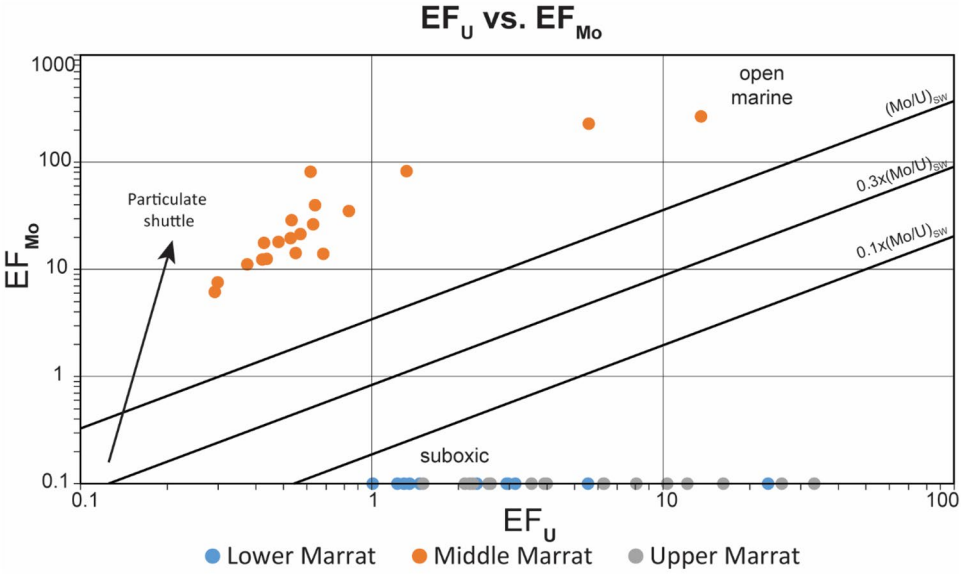

Figure 4. Cross plot of the enrichment factors of Mo and U showing significant enrichment in Mo with no coeval enrichment in U. This trend for the middle Marrat suggests that Mo is likely being scavenged by other phases in the sediment[80,81] .

It is noteworthy that while Al normalization was performed to minimize or remove the lithological effect on the analyzed elemental data and it yields no enrichment in the red beds, it shows significant enrichment of redox-sensitive metals in the overlying and underlying carbonates (Table1). This suggests a potentially anoxic condition during the deposition of the Marrat carbonates, contrary to the overall environmental conditions and interpretation of these carbonates which have been interpreted to form in a well-oxygenated environment, as indicated by their $^{13}C_{org}$ and fossils abundance. This points to the need of a more robust normalization technique to minimize the lithological effect on the redox-sensitive element concentrations and geochemical proxy (e.g., REE and metal isotopes) to unravel the actual physicochemical ocean conditions during depositions of the Marrat carbonates and red beds.

Origin and mechanism of reddening. An early interpretation of the Marrat red beds suggested that the reddening or red pigmentation was caused by the enrichment of hematite due to the laterization of the Arabian shield[82]. The majority of previous works agreed that the reddening process of marine red beds was primarily controlled by the presence of iron oxides[83], with iron being primarily sourced by either continental weathering or biological induction (authigenic precipitation)[22].

Marine red beds are typically reported as deep, basinal deposits formed under oxic conditions following major OAE's, particularly during Cretaceous OAE's[21,22]. Other time periods, including Toarcian, also experienced the development of widespread marine red beds at various time intervals[22,23,84]. Most of these studies interpreted these red beds as basinal deposits that were developed shortly or much later after the T-OAE. In contrast to the deep oceanic red beds, the origin and mechanism of shallow-marine red beds, as in the Marrat Formation, are still much debated. The most widely accepted hypothesis is that shallow-marine red beds developed under oxic conditions, while their counterpart basinal black shale deposits experienced marine anoxia, as illustrated during the Great Ordovician Biodiversification Event[24–26].

The Marrat red beds do not exhibit geochemical signals associated with marine anoxia and increased productivity (Fig. 2), proposing shallow marine oxic conditions for the Marrat. It is highly likely due to the intensified continental weathering during the T-CIE, huge amounts of iron were delievered to the Arabian inner shelf, where dominant oxic conditions cauesed their oxidation. In our proposed model, the Marrat red beds were deposited under shallow-water oxic conditions that were time-equivalent to the deep anoxic conditions associated with the T-OAE (Fig. 5).

Conclusion

The new finding that the middle Marrat deposits are of marine origin provided an opportunity to examine the existence of the Toarcian Carbon Isotope Excursion (T-CIE) in Arabia. Geochemical analyses of the Toarcian Marrat Formation revealed, for the first time, the recognition of the T-CIE in Arabia, which is marked by a distinct negative CIE reported from $\delta^{13}C_{org}$. Furthermore, the increase in various weathering indicators (CIA, PIA, and CIW) suggests elevated CO_2 concentrations in the atmosphere and accelerated continental weathering possibly associated with the widespread T-OAE. The observed geochemical signals within the Marrat red beds propose that they were originally deposited in shallow-marine oxic settings, while the Toarcian oceanic anoxic conditions were dominating the deeper settings.

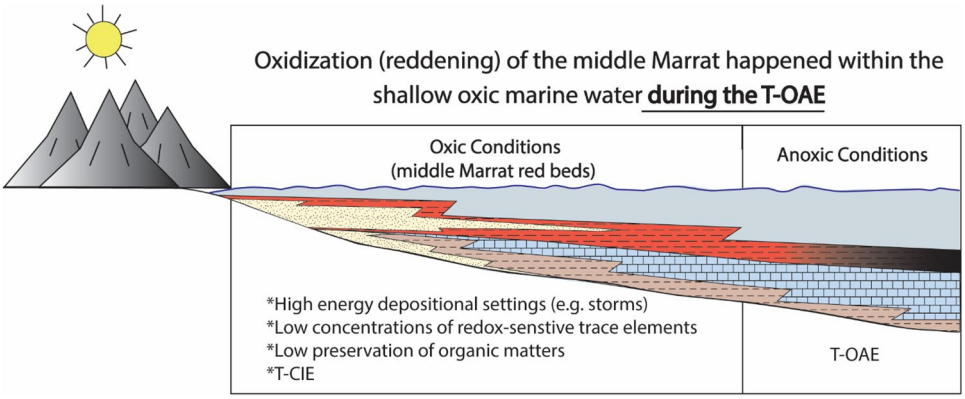

Figure 5. Schematic diagram explaining the proposed model for the middle Marrat red beds, where the redding was possibly taking place in well, oxygenated shallow marine settings ,while the Toarcian oceanic anoxic conditions were dominating the deeper settings.

The first recognition of the T-CIE in Arabia, as highlighted in this study, will significantly contribute to the global understanding of this major event and its geographical extent. Furthermore, it will open the door for future researchers to further investigate the occurrence of T-OAE across the Arabian Plate and its potential impact on the Arabian Jurassic stratigraphy which constitutes one of the most prolific petroleum systems in the world.

Data availability

All data used in this study is presented here and available in the supplementary material. Additional request may be made directly through the corresponding author on reasonable request.

Received: 15 May 2022; Accepted: 30 September 2022
Published online: 27 October 2022

References

1. Jenkyns, H. C. The early toarcian and cenomanian-turonian anoxic events in Europe: comparisons and contrasts. *Geol. Rund.* **74**(3), 505–518. https://doi.org/10.1007/BF01821208 (1985).
2. Jenkyns, H. The early Toarcian (Jurassic) anoxic event-stratigraphic, sedimentary, and geochemical evidence. *Am. J. Sci.* https://doi.org/10.2475/ajs.288.2.101 (1988).
3. Hesselbo, S. P. *et al.* Massive dissociation of gas hydrate during a Jurassic oceanic anoxic event. *Nature* **406**(6794), 392–395. https://doi.org/10.1038/35019044 (2000).
4. Hesselbo, S. P., Jenkyns, H. C., Duarte, L. V. & Oliveira, L. C. Carbon-isotope record of the Early Jurassic (Toarcian) Oceanic Anoxic Event from fossil wood and marine carbonate (Lusitanian Basin, Portugal). *Earth. Plan. Sci. Lett.* **253**(3–4), 455–470. https://doi.org/10.1016/j.epsl.2006.11.009 (2007).
5. Bailey, T. R., Rosenthal, Y., McArthur, J. M., Van de Schootbrugge, B. & Thirlwall, M. F. Paleoceanographic changes of the Late Pliensbachian-Early Toarcian interval: a possible link to the genesis of an Oceanic Anoxic Event. *Earth. Plan. Sci. Lett.* **212**(3–4), 307–320. https://doi.org/10.1016/S0012-821X(03)00278-4 (2003).
6. Cohen, A. S., Coe, A. L. & Kemp, D. B. The Late Palaeocene-Early Eocene and Toarcian (Early Jurassic) carbon isotope excursions: a comparison of their time scales, associated environmental changes, causes and consequences. *J. Geol. Soc.* **164**(6), 1093–1108. https://doi.org/10.1144/0016-76492006-123 (2007).
7. Ruebsam, W., Mayer, B. & Schwark, L. Cryosphere carbon dynamics control early Toarcian global warming and sea level evolution. *Global Planet. Change* **172**, 440–453 (2019).
8. Little, C. T. & Benton, M. J. Early Jurassic mass extinction: a global long-term event. *Geology* **23**(6), 495–498. https://doi.org/10.1130/0091-7613(1995) (1995).
9. Wignall, P. B., Newton, R. J. & Little, C. T. The timing of paleoenvironmental change and cause-and-effect relationships during the Early Jurassic mass extinction in Europe. *Am. J. Sci.* **305**(10), 1014–1032. https://doi.org/10.2475/ajs.305.10.1014 (2005).
10. Jenkyns, H. C., Jones, C. E., Grocke, D. R., Hesselbo, S. P. & Parkinson, D. N. Chemostratigraphy of the Jurassic System: applications, limitations and implications for palaeoceanography. *J. Geol. Soc.* **159**(4), 351–378. https://doi.org/10.1144/0016-764901-130 (2002).
11. Kemp, D. B., Coe, A. L., Cohen, A. S. & Schwark, L. Astronomical pacing of methane release in the Early Jurassic period. *Nature* **437**(7057), 396–399. https://doi.org/10.1038/nature04037 (2005).
12. Them, T. R. II. *et al.* High-resolution carbon isotope records of the Toarcian Oceanic Anoxic Event (Early Jurassic) from North America and implications for the global drivers of the Toarcian carbon cycle. *Earth Planet. Sci. Lett.* **459**, 118–126 (2017).
13. Ruebsam, W., Pieńkowski, G. & Schwark, L. Toarcian climate and carbon cycle perturbations–its impact on sea-level changes, enhanced mobilization and oxidation of fossil organic matter. *Earth Planet. Sci. Lett.* **546**, 116417 (2020).
14. Ruebsam, W., Reolid, M., Marok, A. & Schwark, L. Drivers of benthic extinction during the early Toarcian (Early Jurassic) at the northern Gondwana paleomargin: implications for paleoceanographic conditions. *Earth Sci. Rev.* **203**, 103117 (2020).
15. McElwain, J. C., Wade-Murphy, J. & Hesselbo, S. P. Changes in carbon dioxide during an oceanic anoxic event linked to intrusion into Gondwana coals. *Nature* **435**(7041), 479–482 (2005).
16. Suan, G. *et al.* Secular environmental precursors to Early Toarcian (Jurassic) extreme climate changes. *Earth Planet. Sci. Lett.* **290**(3–4), 448–458 (2010).
17. Al-Suwaidi, A. H. *et al.* First record of the Early Toarcian oceanic anoxic event from the Southern Hemisphere, Neuquén Basin. *Argentina. J. Geol. Soc* **167**(4), 633–636. https://doi.org/10.1144/0016-76492010-025 (2010).
18. Fantasia, A. *et al.* The Toarcian oceanic anoxic event in southwestern Gondwana: an example from the Andean Basin, northern Chile. *J. Geol. Soc.* **175**(6), 883–902. https://doi.org/10.1144/jgs2018-008 (2018).

19. Ruebsam, W. & Al-Husseini, M. Calibrating the Early Toarcian (Early Jurassic) with stratigraphic black holes (SBH). *Gondwana Res.* **82**, 317–336 (2020).
20. Bodin, S. *et al.* Toarcian carbon isotope shifts and nutrient changes from the Northern margin of Gondwana (High Atlas, Morocco, Jurassic): palaeoenvironmental implications. *Palaeogeogr. Palaeoclimatol. Palaeoecol.* **297**(2), 377–390. https://doi.org/10.1016/j.palaeo.2010.08.018 (2010).
21. Wang, C., Hu, X., Sarti, M., Scott, R. W. & Li, X. Upper Cretaceous oceanic red beds in southern Tibet: a major change from anoxic to oxic, deep-sea environments. *Cret. Res.* **26**(1), 21–32. https://doi.org/10.1016/j.cretres.2004.11.010 (2005).
22. Song, H. *et al.* The onset of widespread marine red beds and the evolution of ferruginous oceans. *Nat. Commun.* **8**(1), 399. https://doi.org/10.1038/s41467-017-00502-x (2017).
23. Li, M. *et al.* Early Triassic oceanic red beds coupled with deep sea oxidation in South Tethys. *Sed. Geol.* **391**, 105519. https://doi.org/10.1016/j.sedgeo.2019.105519 (2019).
24. Luan, X. *et al.* Environmental changes revealed by Lower-Middle Ordovician deeper-water marine red beds from the marginal Yangtze Platform, South China: Links to biodiversification. *Palaeogeogr. Palaeoclimatol. Palaeoecol.* **562**, 110116. https://doi.org/10.1016/j.palaeo.2020.110116 (2021).
25. Zhang, X. L. *et al.* Connecting the marine red beds with the onset of the Great Ordovician Biodiversification Event: a case study from the Laojianshan Formation of western Yunnan. *Sibumasu Massif. Palaeoworld* **28**(1–2), 211–223 (2019).
26. McLaughlin, P. I., Emsbo, P. & Brett, C. E. Beyond black shales: the sedimentary and stable isotope records of oceanic anoxic events in a dominantly oxic basin (Silurian; Appalachian Basin, USA). *Palaeogeogr. Palaeoclimatol. Palaeoecol.* **367**, 153–177 (2012).
27. Énay, R., Le Nindre, Y.-M., Mangold, C., Manivit, J., Vaslet, D. Le Jurassique d'Arabie Saoudite centrale: données nouvelles sur les unités lithostratigraphiques, les paléoenvironnements, les faunes d'ammonites, les âges et les corrélations. Geobios, Lyon, Mém. H.S. no. 9, p. 13–65, 5 fig., 2 tabl., 6 pl (1987).
28. Manivit, J., Le Nindre, Y.M. and Vaslet, D. Le Jurassique d'Arabie centrale. Histoire g6ologique de la bordnre occidentale de la plate-forme arabe. Bureau de Recherches Géologiques et Minières report, France (1990).
29. Énay R., Mangold, Ch. Jurassic ammonites from Central Saudi.Arabia (Jebel Tuwaiq and adjacent areas). *Revue de Paléobiologie* **40**(1), 197 (2021).
30. Powers, R.W., Ramirez, L.F., Redmond, C.D. and Elberg, E.L. Geology of the Arabian Peninsula: (p. 147). United States Department of the Interior, Geological Survey (1966).
31. Powers, R. W. *Lexique Stratigraphique International* 483–515 (Centre National de la Recherche Scientifique, 1968).
32. El-Sorogy, A. S., Gameil, M., Youssef, M. & Al-Kahtany, K. M. Stratigraphy and macrofauna of the lower jurassic (toarcian) Marrat Formation, central Saudi Arabia. *J. Afr. Earth Sci.* **134**, 476–492 (2017).
33. Farouk, S., Al-Kahtany, K., El-Sorogy, A. & El-Motaal, E. A. High-frequency cycles and sequence stratigraphy of the lower Jurassic Marrat Formation, central Saudi Arabia. *Mar. Petrol. Geol.* **98**, 369–383 (2018).
34. Al-Mojel, A., Razin, P., Le Nindre, Y. M. & Dera, G. Shallow-marine depositional sequences in a transgressive mixed siliciclastic-carbonate system: the Early Jurassic Marrat Formation from central Saudi Arabia. *J. Afr. Earth. Sci.* **167**, 103429. https://doi.org/10.1016/j.jafrearsci.2019.02.011 (2020).
35. Al-Hussaini, A., Alnazghah, M., Al-Ramadan, K., Fallatah, M. & Polo, C. Asymmetrical wave-dominated siliciclastic shorelines with evidence of along-strike variability of sedimentary processes: a revised interpretation for the Toarcian Marrat red beds, central Arabia. *Mar. Pet. Geol.* **126**, 104915. https://doi.org/10.1016/j.marpetgeo.2021.104915 (2021).
36. Beydoun, Z. R. *Arabian Plate Hydrocarbon Geology and Potential: A Plate Tectonic Approach*. AAPG Bull., Tulsa, OK (1991).
37. Ziegler, M. A. Late permian to holocene paleofacies evolution of the Arabian Plate and its hydrocarbon occurrences. *GeoArabia* **6**, 445–504 (2001).
38. Sharland, P. R., Archer, R., Casey, D. M., Hall, R. B. D. S. H., Heward, A. P., Horbury, A. D., Simmons, M. D. Arabian Plate Sequence Stratigraphy. GeoArabia Spec. Pub., vol. 2. Gulf PetroLink, Bahrain (2001).
39. Manivit, J., Pellaton, C., Vaslet, D., Le Nindre, Y.M., Brosse, J.M., Fourniguet, J. Explanatory notes to the geologic map of the wadi Al mulayh quadrangle, kingdom of Saudi Arabia. *Geoscience Map GM-92C*, scale 1 (250,000) (1985a).
40. Manivit, J., Pellaton, C., Vaslet, D., Le Nindre, Y.M., Brosse, J.M., Breton, J.P., Fourniguet, J., Prevot, J. C. Explanatory notes to the geologic map of the Darma'Quadrangle, kingdom of Saudi Arabia. *Geoscience map GM-101C*, scale 1 (250,000) (1985b).
41. Al-Hussaini, A. *et al.* New evidence of regressing and transgressing Jurassic siliciclastic coastlines within the Dhruma Formation in Northern Central Arabia, Saudi Arabia. *Sed. Geol.* **379**, 114–137 (2019).
42. Le Nindre, Y. M., Manivit, J., Manivit, H. & Vaslet, D. Stratigraphie sequentielle du Jurassique et du Cretace en Arabie Saoudite. *Bull. Soc. Geol. Fr.* **6**(6), 1025–1034 (1990).
43. Al-Husseini, M. I. Jurassic sequence stratigraphy of the western and southern Arabian Gulf. *GeoArabia* **2**(4), 361–382 (1997).
44. Vaslet, D., Brosse, J. M., Breton, J. P., Manivit, J., Le Strat, P., Fourniguet, J., Shorbaji, H. Explanatory notes to the geologic map of the Shaqra quadrangle, kingdom of Saudi Arabia. *Geoscience map GM-120C*, scale 1 (250,000) (1988).
45. Vaslet, D., Manivit, J., Le Nindre, Y. M., Brosse, J. M., Fourniguet, J., Delfour, J. Explanatory notes to the geological map of the Wadi ar Rayn quadrangle, sheet 23H, Kingdom of Saudi Arabia. Saudi Arabian Deputy Ministry for Mineral Resources Geoscience map GM-63A, Scale 1 (250,000), 17–19 (1983).
46. Le Nindre, Y. M., Vaslet, D., Manivit, J. H. and Al-Husseini, M. I. Sequence architecture of the Toarcian Marrat Formation, Saudi Arabia: the Khashm adh Dhibi reference section (2022).
47. Arkell, W. J., Bramkamp, R. A., Steineke, M. Jurassic ammonites from Jebel Tuwaiq, central Arabia with stratigraphical introduction. *Philos. Trans. R. Soc. Lond. B Biol. Sci.* **236**(633), 241–314 (1952).
48. Koeshidayatullah, A. *et al.* Evaluating new fault-controlled hydrothermal dolomitization models: Insights from the Cambrian Dolomite Western Canadian Sedimentary Basin. *Sedimentology sed.* 12729 https://doi.org/10.1111/sed.12729.
49. Stacey, J., Hollis, C., Corlett, H. & Koeshidayatullah, A. Burial dolomitization driven by modified seawater and basal aquifer-sourced brines: Insights from the Middle and Upper Devonian of the Western Canadian Sedimentary Basin. *Basin Res.* **33**(1), 648–680. https://doi.org/10.1111/bre.12489 (2021).
50. Tribovillard, N., Algeo, T. J., Lyons, T. & Riboulleau, A. Trace metals as paleoredox and paleoproductivity proxies: an update. *Chem. Geol.* **232**(1–2), 12–32 (2006).
51. Turekian, K. K. & Wedepohl, K. H. Distribution of the elements in some major units of the earth's crust. *Geol. Soc. Am. Bull.* **72**(2), 175–192 (1961).
52. Nesbitt, H., Young, G. M. Early Proterozoic climates and plate motions inferred from major element chemistry of lutites. *Nature*, **299**(5885), 715–717 (1982).
53. Harnois, L. The CIW index: a new chemical index of weathering. *Sed. Geol.* **55**(3), 319–322 (1988).
54. Fedo, C. M., Wayne Nesbitt, H. & Young, G. M. Unraveling the effects of potassium metasomatism in sedimentary rocks and paleosols, with implications for paleoweathering conditions and provenance. *Geology* **23**(10), 921–924 (1995).
55. van de Schootbrugge, B. *et al.* The Schandelah Scientific Drilling Project: A 25-million-year record of Early Jurassic palaeoenvironmental change from northern Germany. *News. Strat.* **52**(3), 249–296. https://doi.org/10.1127/nos/2018/0259 (2019).
56. Krencker, F. N. *et al.* Two-phased collapse of the shallow-water carbonate factory during the late Pliensbachian-Toarcian driven by changing climate and enhanced continental weathering in the Northwestern Gondwana Margin. *Earth Sci. Rev.* **208**, 103254 (2020).

57. Ruebsam, W., Reolid, M., Mattioli, E. & Schwark, L. Organic carbon accumulation at the northern Gondwana paleomargin (Tunisia) during the Toarcian Oceanic Anoxic Event: Sedimentological and geochemical evidence. *Palaeogeogr. Palaeoclimatol. Palaeoecol.* **586**, 110781 (2022).
58. Cohen, A. S., Coe, A. L., Harding, S. M. & Schwark, L. Osmium isotope evidence for the regulation of atmospheric CO2 by continental weathering. *Geology* **32**(2), 157–160 (2004).
59. Jenkyns, H. C., Gröcke, D. R. & Hesselbo, S. P. Nitrogen isotope evidence for water mass denitrification during the early Toarcian (Jurassic) oceanic anoxic event. *Paleoceanography* **16**(6), 593–603 (2001).
60. Schouten, S., van Kaam-Peters, H. M., Rijpstra, W. I. C., Schoell, M. & Damste, J. S. S. Effects of an oceanic anoxic event on the stable carbon isotopic composition of early Toarcian carbon. *Am. J. Sci.* **300**(1), 1–22 (2000).
61. Hu, X., Li, J., Han, Z. & Li, Y. Two types of hyperthermal events in the Mesozoic-Cenozoic: environmental impacts, biotic effects, and driving mechanisms. *Sci. China Earth. Sci.* **63**(8), 1041–1058. https://doi.org/10.1007/s11430-019-9604-4 (2020).
62. Damborenea, S. E. Jurassic evolution of Southern Hemisphere marine palaeobiogeographic units based on benthonic bivalves. *Geobios* **35**(24), 51–71. https://doi.org/10.1016/S0016-6995(02)00048-7 (2002).
63. Gröcke, D. R., Hori, R. S., Trabucho-Alexandre, J., Kemp, D. B. & Schwark, L. An open ocean record of the Toarcian oceanic anoxic event. *Sol. Earth* **2**(2), 245–257. https://doi.org/10.5194/se-2-245-2011 (2011).
64. Littler, K., Hesselbo, S. P. & Jenkyns, H. C. A carbon-isotope perturbation at the Pliensbachian–Toarcian boundary: evidence from the Lias Group NE England. *Geol Mag.* **147**(2), 181–192. https://doi.org/10.1017/S0016756809990458 (2010).
65. Fu, X. *et al.* Continental weathering and palaeoclimatic changes through the onset of the Early Toarcian oceanic anoxic event in the Qiangtang Basin, eastern Tethys. Palaeo. Palaeo. *Palaeo.* **487**, 241–250. https://doi.org/10.1016/j.palaeo.2017.09.005 (2017).
66. Lyons, T. W., Werne, J. P., Hollander, D. J. & Murray, R. W. Contrasting sulfur geochemistry and Fe/Al and Mo/Al ratios across the last oxic-to-anoxic transition in the Cariaco Basin. *Venezuela. Chem. Geol.* **195**, 131–157 (2003).
67. Sageman, B. B. *et al.* A tale of shales: the relative roles of production, decomposition, and dilution in the accumulation of organic-rich strata, Middle-Upper Devonian, Appalachian Basin. *Chem. Geol.* **195**, 229–273 (2003).
68. Rimmer, S. M. Geochemical paleoredox indicators in Devonian– Mississippian black shales, Central Appalachian Basin (USA). *Chem. Geol.* **206**, 373–391 (2004).
69. Algeo, T. J. & Maynard, J. B. Trace-element behavior and redox facies in core shales of Upper Pennsylvanian Kansas-type cyclothems. *Chem. Geol.* **206**, 289–318 (2004).
70. Algeo, T. J. Can marine anoxic events draw down the traceelement inventory of seawater?. *Geology* **32**, 1057–1060 (2004).
71. Nameroff, T.J., Calvert, S.E., Murray, J. W. Glacial-interglacial variability in the eastern tropical North Pacific oxygen minimum zone recorded by redox-sensitive trace metals. *Paleoceanography* **19**, PA1010 (2004). doi:https://doi.org/10.1029/2003PA000912.
72. Tribovillard, N., Averbuch, O., Devleeschouwer, X., Racki, G. & Riboulleau, A. Deep-water anoxia over the Frasnian– Famennian boundary (La Serre, France): a tectonically-induced oceanic anoxic event?. *Terra Nova* **16**, 288–295 (2004).
73. Tribovillard, N., Ramdani, A., Trentesaux, A. Controls on organic accumulation in Late Jurassic shales of northwestern Europe as inferred from trace-metal geochemistry. In: Harris, N. (Ed.*), The Deposition of Organic-Carbon-Rich Sediments: Models, Mechanisms, and Consequences*. SEPM Spec. Public., vol. 82, pp. 145–164 (2005).
74. Riquier, L., Tribovillard, N., Averbuch, O., Joachimski, M.M., Racki, G., Devleeschouwer, X., El Albani, A., Riboulleau, A. Productivity and bottom water redox conditions at the Frasnian–Famennian boundary on both sides of the Eovariscan Belt: constraints from trace-element geochemistry. In: Over, D.J., Morrow, J.R., Wignall, P.B. (Eds.), *Understanding Late Devonian and Permian–Triassic Biotic and Climatic Events: Towards an Integrated Approach: Developments in Palaeontology and Stratigraphy*. Elsevier Pub. Co., pp. 199–224 (2005).
75. Erba, E. *et al.* Environmental consequences of Ontong Java Plateau and Kerguelen plateau volcanism. The origin, evolution, and environmental impact of oceanic large igneous provinces. *Geol. Soc. Am. Spec. Pap.* **511**, 271–303 (2015).
76. Jenkyns, H. C. Transient cooling episodes during Cretaceous Oceanic Anoxic Events with special reference to OAE 1a (Early Aptian). *Philos. Trans. R. Soc. A: Math. Phys. Eng. Sci.* **376**(2130), 20170073 (2018).
77. Jenkyns, H. C., Dickson, A. J., Ruhl, M. & Van den Boorn, S. H. Basalt-seawater interaction, the Plenus Cold Event, enhanced weathering and geochemical change: deconstructing Oceanic Anoxic Event 2 (Cenomanian–Turonian, Late Cretaceous). *Sedimentology* **64**(1), 16–43 (2017).
78. Fantasia, A. *et al.* Global versus local processes during the Pliensbachian-Toarcian transition at the Peniche GSSP, Portugal: a multi-proxy record. *Earth Sci. Rev.* **198**, 102932 (2019).
79. Algeo, T. J. & Tribovillard, N. Environmental analysis of paleoceanographic systems based on molybdenum–uranium covariation. *Chem. Geol.* **268**(3–4), 211–225 (2009).
80. Morford, J. L. & Emerson, S. The geochemistry of redox sensitive trace metals in sediments. *Geochim. Cosmochim. Acta* **63**(11–12), 1735–1750 (1999).
81. Morford, J. L., Emerson, S. R., Breckel, E. J. & Kim, S. H. Diagenesis of oxyanions (V, U, Re, and Mo) in pore waters and sediments from a continental margin. *Geochim. Cosmochim. Acta* **69**(21), 5021–5032 (2005).
82. Abed, A. M. Lower Jurassic lateritic redbeds from central Arabia. *Sed. Geol.* **24**(1–2), 149–156. https://doi.org/10.1016/0037-0738(79)90034-4 (1979).
83. McBride, E. F. Significance of color in red, green, purple, olive, brown, and gray beds of Difunta Group, northeastern Mexico. *J. Sed. Res.* **44**(3), 760–773. https://doi.org/10.1306/212F6B9A-2B24-11D7-8648000102C1865D (1974).
84. Schröder, S., Bedorf, D., Beukes, N. J. & Gutzmer, J. From BIF to red beds: Sedimentology and sequence stratigraphy of the Paleoproterozoic Koegas Subgroup (South Africa). *Sed. Geol.* **236**(1–2), 25–44. https://doi.org/10.1016/j.sedgeo.2010.11.007 (2011).

Acknowledgements

We acknowledged the support from KFUPM for the fieldwork and geochemical analysis through the startup funds (SF19003 and SF21011). We appreciate the constructive comment from Hugh Jenkyns and Dan Lehrmann on the earlier version of this manuscript. HS was funded by the National Natural Science Foundation of China (Grant 92155201).

Author contributions

M.A.: Conceptualization, Methodology, Writing—original draft, Data curation, Writing—review & editing. A.K.: Writing—original draft, Data curation, Writing—review & editing. A.A.-H.: Conceptualization, Discussion, Writing—review & editing, A.A.: Analysis, Writing—review & editing. H.S.: Discussion, Writing—review & editing. K.A.-R.: Discussion, Writing—review & editing. All authors reviewed the manuscript.

Competing interests

The authors declare no competing interests.

Additional information

Supplementary Information The online version contains supplementary material available at https://doi.org/10.1038/s41598-022-21716-0.

Correspondence and requests for materials should be addressed to A.K.

Reprints and permissions information is available at www.nature.com/reprints.

Publisher's note Springer Nature remains neutral with regard to jurisdictional claims in published maps and institutional affiliations.